

# Partial Topological Protection in $C_4$ Lattices for Optical Communications

Ondřej Novák,<sup>1, a)</sup> Gervasi Herranz,<sup>2</sup> and Martin Veis<sup>1</sup>

<sup>1)</sup>Charles University, Faculty of Mathematics and Physics, Ke Karlovu 5, 121 16 Prague, Czech Republic

<sup>2)</sup>Institut de Ciència de Materials de Barcelona (ICMAB-CSIC), Campus UAB, 08193 Bellaterra, Catalonia, Spain

(\*Electronic mail: ondrej.novak@matfyz.cuni.cz)

(Dated: 18 February 2025)

In recent studies, analogs of the electronic Quantum Spin-Hall Effect have been explored within photonic crystals that incorporate spatial symmetries, especially those with  $C_{6v}$  symmetry, where  $\mathbb{Z}_2$  topological invariants are enforced by crystalline symmetry. These photonic crystals possess bulk states with well-defined pseudospins and exhibit helical edge states, closely resembling their electronic counterparts. However, achieving  $\mathbb{Z}_2$  topological protection in a square lattice photonic crystal remains a great theoretical and experimental challenge. In this work, we propose a single material photonic crystal structure based on a  $C_4$  lattice that supports partially  $\mathbb{Z}_2$ -protected edge modes. We show that this structure can host a photonic band-gap that hosts  $\mathbb{Z}_2$ -like modes, enabling perfect transmission in waveguide applications. Furthermore, we investigate the robustness of these modes against structural defects and directional turns, highlighting the distinctions between full  $\mathbb{Z}_2$  topological protection and partial topological protection. Finally, we analyze the impact of the number of elementary cells surrounding the interface on the formation and stability of these protected modes.

## I. INTRODUCTION

Over the past decade, the field of topological protection in photonics has witnessed significant growth and sustained interest<sup>5,8,24,29,33,38,40,43,44,56</sup>. The most promising applications of topologically protected states of light are emerging in optical insulators<sup>16,41</sup>, topological waveguides and couplers<sup>7,10,15,17,20–22,52</sup>, as well as in topological lasers<sup>9</sup>, on-chip nanobeam filters<sup>27</sup>, wavelength-division multiplexing<sup>11</sup>, logic gates<sup>54</sup>, and other cutting-edge photonic applications. Fabrication<sup>34</sup> and characterization technologies<sup>2,23,25,28,35,37,47,53</sup> are becoming well-established, with increasing efforts to ensure compatibility with integrated photonic platforms<sup>21</sup>.

The primary property of interest in most cases is the suppression of back-scattering in topologically protected edge modes, enabling lossless transmission even in the presence of defects or sharp turns<sup>4,6,13,26,45,48,50,51</sup>. Despite considerable advancements in the field, exploring additional geometric lattice configurations remains valuable for specific applications, such as logic gates, where the photonic crystal (PC) lattice determines the available turns and influences integration density<sup>12</sup>. In the  $C_4$  lattice, only Chern topological protection<sup>40</sup> and valley-Chern protection<sup>15</sup> have been achieved, but not full  $\mathbb{Z}_2$  protection. Chern insulators are typically limited to radio frequencies due to the insufficient off-diagonal permeability in other spectral regions<sup>31,42</sup>, a necessary condition for breaking time-reversal symmetry. Valley-Chern topology operates without breaking time-reversal symmetry but is constrained to half of the Brillouin zone. By contrast,  $\mathbb{Z}_2$  topology avoids these limitations, making it the preferred solution if achievable.

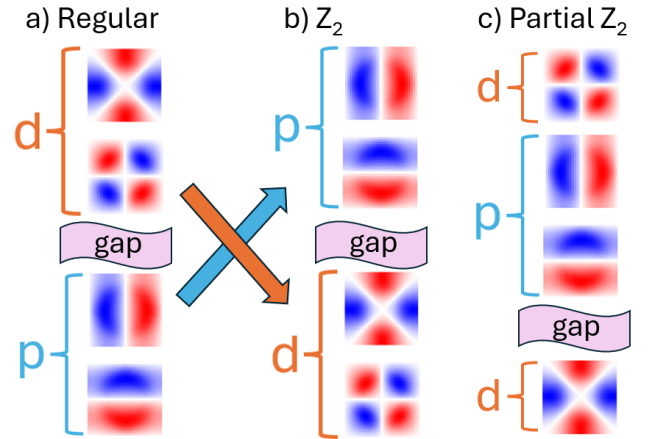


FIG. 1. Schematic depiction of band symmetry ordering. a) Non-inverted band ordering, showing the field distribution of eigenstates at the  $\Gamma$  point, where the  $d$ -states lie at a higher energy than the  $p$ -states. b) Inverted band structure, where the  $d$ -states are lower in energy than the  $p$ -states. When this inverted band structure is fully gapped and interfaces with a non-inverted band structure, it results in a  $\mathbb{Z}_2$  topologically protected state, enabling the photonic Quantum Spin Hall Effect. c) Partial inversion, where only one of the two  $d$ -states lies below the  $p$ -states and is gapped. This is the configuration explored in this study. For a more detailed discussion of eigenstates, please refer to Sec. IA.

Achieving  $\mathbb{Z}_2$  topological protection in the  $C_4$  lattice is highly desirable due to its compatibility with orthogonal logic, which is the standard approach in modern processors<sup>36</sup>. Orthogonal implementations inherently allow for more efficient space usage, as they simplify routing and minimize parasitic effects, crucial for high-density photonic integration. Moreover, the symmetry of the  $C_4$  lattice facilitates straightforward and compact designs for logic gates and devices, making it more convenient for both fabrication and integration into com-

<sup>a)</sup> Also at Institut de Ciència de Materials de Barcelona (ICMAB-CSIC), Campus UAB, 08193 Bellaterra, Catalonia, Spain

plex photonic circuits. These advantages position the  $C_4$  lattice as a practical and versatile platform for advancing topological photonics.

In this paper, we present the realization of partial  $\mathbb{Z}_2$  topological protection in a  $C_4$  lattice using a single material (see Fig. 1). We analyze both the aspects of topological protection that are preserved and those that are compromised. Several studies have investigated partial  $\mathbb{Z}_2$  topological protection in  $C_4$  lattices. For instance He et al.<sup>12</sup> reported transmission reached approximately 95% over 7.5  $\mu\text{m}$ , which does not indicate robust topological protection compared to the 100% transmission demonstrated in our study. Another approach, described by Xiong et al.<sup>49</sup>, employed multiple materials, significantly increasing the complexity of the fabrication process. More recently, Zhang et al.<sup>55</sup> utilized a Penrose-square photonic crystal, which is considerably more complex to fabricate than our design. Moreover, their implementation relies on unusually high permittivity, which is typically difficult to achieve in a spectral region without absorption.

In contrast, our design builds on a simple unit cell that is straightforward to fabricate and is based on InP, which has near-ideal optical properties at the target wavelength of 1550 nm. InP is widely used in photonics and is well suited for lithographic preparation.

### A. Photonic eigenproblem

Topological invariants of photonic systems can be derived from Maxwell's equations. In two dimensions, these equations decouple into transverse electric (TE) and transverse magnetic (TM) modes<sup>19</sup>. Here, we focus on TM modes, allowing us to formulate a wave equation for the  $z$ -component of the electric field:

$$\nabla \times \nabla \times \mathbf{E}_z(\mathbf{r}) = \left(\frac{\omega}{c}\right)^2 \boldsymbol{\varepsilon}(\mathbf{r})\mathbf{E}_z(\mathbf{r}), \quad (1)$$

where  $\boldsymbol{\varepsilon}(\mathbf{r})$  represents a spatially and possibly frequency-dependent dielectric tensor. This wave equation can be framed as an eigenvalue problem:

$$\hat{A}E_z(\mathbf{r}) = aE_z(\mathbf{r}), \quad (2)$$

where  $\hat{A}$  is an operator acting on  $E_z$ , with eigenvalue  $a$ . These eigenvalues form energy bands, and in general,  $\hat{A}$  has an infinite number of eigenvalues; however, we focus only on the lowest few. We express eigenvalues in reduced units,  $\frac{\omega a}{2\pi c}$ , equivalent to  $\frac{a}{\lambda}$ , where  $a$  denotes the lattice parameter. Given the periodicity of  $\boldsymbol{\varepsilon}(\mathbf{r})$ , Bloch's theorem allows us to isolate the periodic component of  $E_z$ <sup>4,46</sup>.

$$E_{z,k}(\mathbf{r}) = e^{i\mathbf{k}\cdot\mathbf{r}}u_k(\mathbf{r}), \quad (3)$$

where  $\mathbf{k}$  is a reciprocal vector.

The primary focus of this paper is the function  $u_k(\mathbf{r})$ , which we obtain using the MPB software package<sup>18</sup>.  $u_k(\mathbf{r})$  is a complex function, so to compare the fields and visualize them, we use the real part with a fixed phase option provided by MPB. Alternative solvers, such as COMSOL or FDTD methods<sup>14,32,39</sup>, could also be used to achieve similar results. For further details on MPB calculations, please refer to appendix A. Although  $u_k(\mathbf{r})$  technically represents only the periodic component of the eigenmodes, we will refer to  $u_k(\mathbf{r})$  as the eigenmode or the Bloch function throughout this paper.

### B. Eigenfunctions

To achieve  $\mathbb{Z}_2$  topological protection, the natural ordering of energy bands in a photonic crystal must reverse due to structural design (analogous to the effects of spin-orbit coupling in electronic systems), where states that typically occupy higher energies descend below lower-energy states (Fig. 1). In photonic systems, if the symmetry and material parameters are tuned to allow for this inversion at certain points, such as the  $\Gamma$  point in the Brillouin zone, it can result in states with non-trivial topological properties, such as the Quantum Spin Hall Effect<sup>3,30</sup>. This effect is characterized by the formation of counter-propagating edge states that carry opposite spins or pseudo-spins and are robust against backscattering from defects. By interfacing a band non-inverted crystal with a band-inverted crystal, a topological interface is created, enabling  $\mathbb{Z}_2$ -protected topological modes in the common band-gap.

A crucial step in designing  $\mathbb{Z}_2$  topological photonic crystals is determining the energy band structure and symmetries of the spatial electric field distributions for different eigenmodes. The spatial electric field distribution of the eigenmodes at the  $\Gamma$  point in the Brillouin zone exhibits symmetry similar to atomic orbitals, allowing classification into types such as  $s$ ,  $p$ ,  $d$ ,  $f$ , etc. For simplicity, we focus here on the  $p$  and  $d$  eigenmode symmetries. Both  $p$  and  $d$  states appear in pairs, and in our dataset, we identify two forms of  $p$  states with symmetries:  $p_1 : x; y$  and  $p_2 : x - y; x + y$ . The  $d$  states are observed as  $d : xy; x^2 - y^2$ . In Fig. 1, we show the electric field distributions of the  $p$  and  $d$  states computed at the  $\Gamma$  point.

## II. STRUCTURE DEFINITION AND SEED BAND-STRUCTURE

To achieve partial  $\mathbb{Z}_2$  topological protection, we start from the structure proposed in Figure 2, which represents an elementary cell of a 2D photonic crystal consisting of indium phosphide InP and air<sup>1</sup>. In practical applications, this pattern would be realized as pillars on a substrate, a method that is already commonly employed<sup>2,25,28,35,47,53</sup>. The pattern is parameterized by  $r_{1-3}$ , where  $r_{1,2}$  define a ring that enforces the  $C_4$  lattice symmetry, and  $r_3$  controls the material-field overlap for the  $d_{x^2-y^2}$  mode. An illustration of a topological interface is shown in Figure 2c.

Dirac-like dispersion in the photonic crystal structure is essential for achieving band inversion, which is sensitive to per-

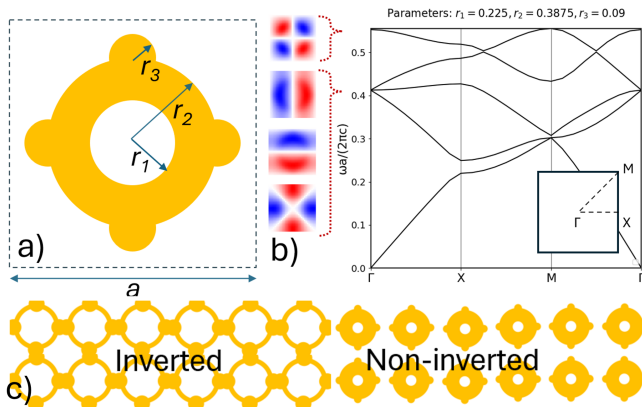


FIG. 2. a) Geometrical definition of the 2D photonic crystal unit cell. The lattice constant is denoted by  $a$ . The orange region represents the InP material in air. The parameters  $r_1$ ,  $r_2$ , and  $r_3$  are variable. Note that the centers of the outer cylinders are positioned at the edge of the inner ring. b) Band structure of a closed-gap geometric configuration defined in Figure 2a. c) Illustration of two semi-infinite photonic crystals forming an interface.

turbations such as inversion symmetry breaking. These perturbations can open a gap and induce  $\mathbb{Z}_2$  topological modes, akin to those found in honeycomb lattices<sup>13</sup>. Starting from the proposed elementary unit cell illustrated in Figure 2, we modulated the geometric parameters to achieve Dirac points in the band structure. However, despite varying the parameters  $r_{1-3}$ , we were unable to identify a combination that would yield a double-Dirac cone. This problem persists in the literature as well. Instead, we focused on a seed state characterized by a Dirac cone with an additional mode traversing it, as depicted in Figure 2b. This figure shows a triple degeneracy at the  $\Gamma$  point, involving both  $p$ -like eigenfunctions and one of the  $d$ -like eigenfunctions. Consequently, when we open the gap by further adjusting the geometry, we will not be able to position both  $d$  states below the  $p$  states. Instead, we will explore the properties of the state shown in Figure 1c, where partial band inversion is achieved. We will demonstrate that this configuration leads to partially protected topological modes in the  $C_4$  lattice.

Once the combination of  $r_{1-3}$  parameters that leads to the topologically inverted state of PC is identified, the next step is to find a non-inverted combination that overlaps with the bandgap around which the inversion occurs. The topological modes are formed within the inverted states, so if no other states are present within the overlapping bandgap, the topological modes can be effectively isolated, enabling precise control of light. In our case, since the configuration space of  $r_{1-3}$  was explored while searching for the inversion, we can directly select the best bandgap overlap case from the non-inverted set of results.

### III. RESULTS

We center our investigation on topological photonic interface formed by interfacing a crystal with a regular, non-

inverted band structure, with another exhibiting band inversion. To identify suitable configurations, we first explored the parameter space to establish regions where the crystals exhibit either regular or inverted-band structures. Figure 3a shows the band structures of both crystal types in the same plot: the bands corresponding to the regular, non-inverted band structure are represented by solid red lines (defined by the elementary cell parameters  $r_1 = 0.105a$ ,  $r_2 = 0.35a$ ,  $r_3 = 0.072a$ ), while the bands for the inverted-band structure (defined by  $r_1 = 0.345a$ ,  $r_2 = 0.425a$ ,  $r_3 = 0.108a$ ) are shown as solid blue lines. We use units of  $a$  (lattice parameter) since the phenomenon is scaleable as long as the material model holds. To determine the value of  $a$ , we select a wavelength we want to target, 1550nm in our case and we look at the highest dispersion of the topological modes at fig. 3b, which is at  $\frac{\omega a}{2\pi c} = 0.42$ . This gives us the value of  $a = 651\text{nm}$ .

We subsequently computed a supercell consisting of 16 unit cells of the regular-band structure crystal interfaced with 16 unit cells of the inverted-band structure crystal. The resulting computed band structure reveals topological edge modes, depicted by the solid magenta line in Figure 3b. These topological modes, appearing in the band gap, exhibit normal dispersion, as seen in the transmission plot in Figure 3b (left). Here, the mode shows approximately 100% transmission (Based on energy flow in FDTD simulation of a large section of the interface, see B) and is surrounded by regions with negligible transmission, which corresponds to the photonic band-gap. This effect is characteristic of  $\mathbb{Z}_2$  topological protection.

The noise observed in the transmission plot is due to the Finite-difference time-domain (FDTD) method, which employs a Fourier transform to capture the spectral response from a time-dependent pulse. Because the simulation time window is finite, oscillatory errors arise, particularly in transmission calculations where oscillations in the denominator significantly affect the result<sup>39</sup>. This issue is more pronounced in Figure 4e, where some transmission values exceed 100%. In these cases, we interpret the data qualitatively rather than quantitatively. For more details on the FDTD simulations, please refer to appendix B.

Our simulations demonstrate that the combination of topologically inverted and non-inverted patterns produces a pair of modes within the common photonic bandgap, characterized by high transmission. The question remains whether partial protection can achieve the same defect-induced robustness and tunability as full  $\mathbb{Z}_2$  topological protection, which we discuss in the next section.

#### A. Mode robustness

Although the topological modes lie in a photonic band gap—thereby prohibiting interaction with bulk states—our simulations show that certain geometric modifications at the interface can still reduce transmission. Specifically, defects or bends placed on one side of the interface tend to disrupt the edge mode more than those on the other side. This asymmetry stands in contrast to the behavior of a fully  $\mathbb{Z}_2$ -protected system, in which any such modifications would not disturb the

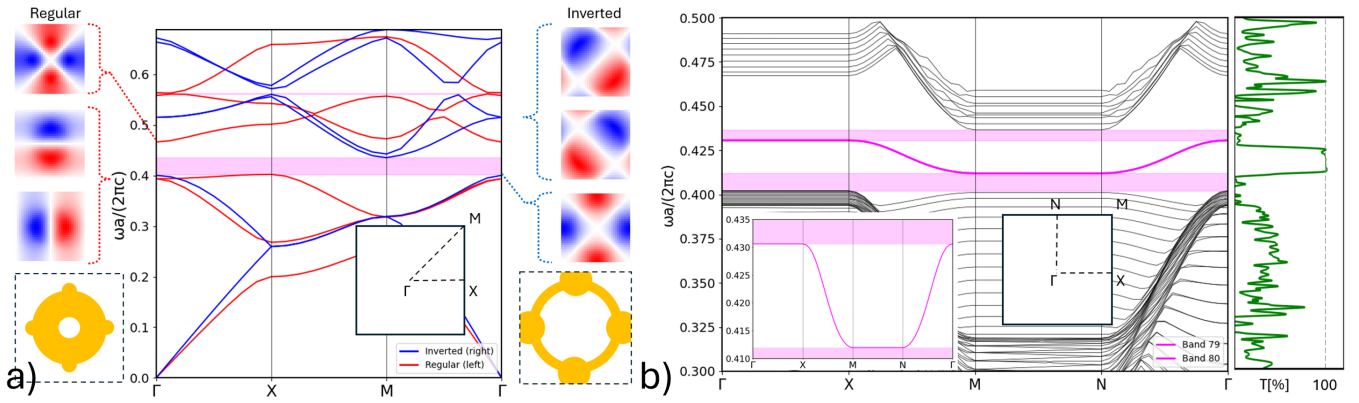


FIG. 3. a) Photonic band-structures obtained for crystals designed according to elementary cells defined in Figure 2. The regular (non-inverted band structure, solid red line) crystal is defined according to parameters:  $r_1 = 0.105a$ ,  $r_2 = 0.35a$ ,  $r_3 = 0.072a$ , while the band-inverted photonic crystal (solid blue line) is defined by parameters  $r_1 = 0.345a$ ,  $r_2 = 0.425a$ ,  $r_3 = 0.108a$ . The band structures of both crystals are overlaid to emphasize the overlapping band-gap and the ordering of eigenfunctions shown as the red and blue field distributions around the figure (see section IA). The broad pink strip represents the band-gap common for both designs. b) Band-structure of a super-cell consisting of sixteen horizontally stacked regular cells and sixteen band-inverted cells. The broad-pink strip represents the original band-gap from 3a. In this band-gap, the solid magenta lines correspond to the topological modes. The green line is a spectral dependence of transmission calculated by FDTD method.

edge mode regardless of their placement. Thus, as discussed in the following, the observed behavior suggests a ‘partial’ topological protection.

To investigate this phenomenon, we conducted two sets of simulations using the FDTD method with the Lumerical solver, as shown in Figure 4. We used 54 spatial steps per PC unit cell in the simulation. Further increases in mesh accuracy were unnecessary, as the results had already converged.

In the first set of simulations, the interface was shaped into either a left or right turn, with the simulation region spanning 40 by 40 unit cells. The field distribution is depicted in Figures 4a,c, where the black and white maps represent inverted and non-inverted elementary cells, respectively.

In the second set, we introduced a pronounced defect within a 20-by-25-unit-cell domain: one cell away from the interface, a line of three consecutive unit cells was swapped from inverted to non-inverted crystal type, or vice versa. The field distribution, along with the unit cell types (black indicating inverted), is depicted in Figures 4b,d. This drastic modification ensures that any sensitivity of the edge mode to localized geometry is clearly visible.

In both cases, right-side modifications consistently preserved near-100% transmission, whereas left-side changes introduced scattering and reduced overall transmission. The transmission is depicted in Figure 4e. Because the modes are confined to a frequency range within the photonic band gap, the absence of bulk states to couple with suggests that these disturbances arise primarily from local boundary effects. These findings confirm that while band-gap isolation prevents bulk scattering, certain symmetries essential for full topological immunity are absent in this partial  $\mathbb{Z}_2$  regime.

A plausible hypothesis for the left–right discrepancy is that local symmetry breaking at the interface, or an intrinsic ‘handedness’ of the design, makes one side more susceptible to perturbations. Although the topological modes do not

couple to bulk states, large local changes—such as swapping multiple cells—can still alter the boundary conditions enough to induce scattering when the mode encounters that region. In contrast, any defect that preserves the interface symmetry (for instance, by being replicated on both sides in a perfectly uniform way) does not disturb the edge mode significantly, as the necessary symmetry for propagation remains intact. Consequently, while these photonic modes exhibit many of the desirable properties of topological edge states, their partial nature allows certain side-specific defects to compromise the otherwise unidirectional flow.

## B. Cell-count effect

One critical parameter often overlooked in photonic topological interface designs is the number of photonic crystal (PC) periods surrounding the interface. This parameter determines how strongly the topological modes localize around the interface and, consequently, how effectively unidirectional propagation is achieved.

In the topological regime, there are two modes, each responsible for transport in one direction, analogous to spin up and spin down in the quantum spin Hall effect. To quantify the field localization and determine the proportion of energy traveling in each direction, the supercell is divided into two regions, each surrounding one of the two interfaces. The Bloch mode  $u_k$  is then integrated in these regions to reveal which interface supports the majority of the mode.

Figure 5a shows that with 10 periods, 99.7% of the energy is confined to one interface, enabling nearly unidirectional transport. Meanwhile, the other mode carries energy in the opposite direction. As the number of PC cells increases, the mode becomes more localized around a single interface. For

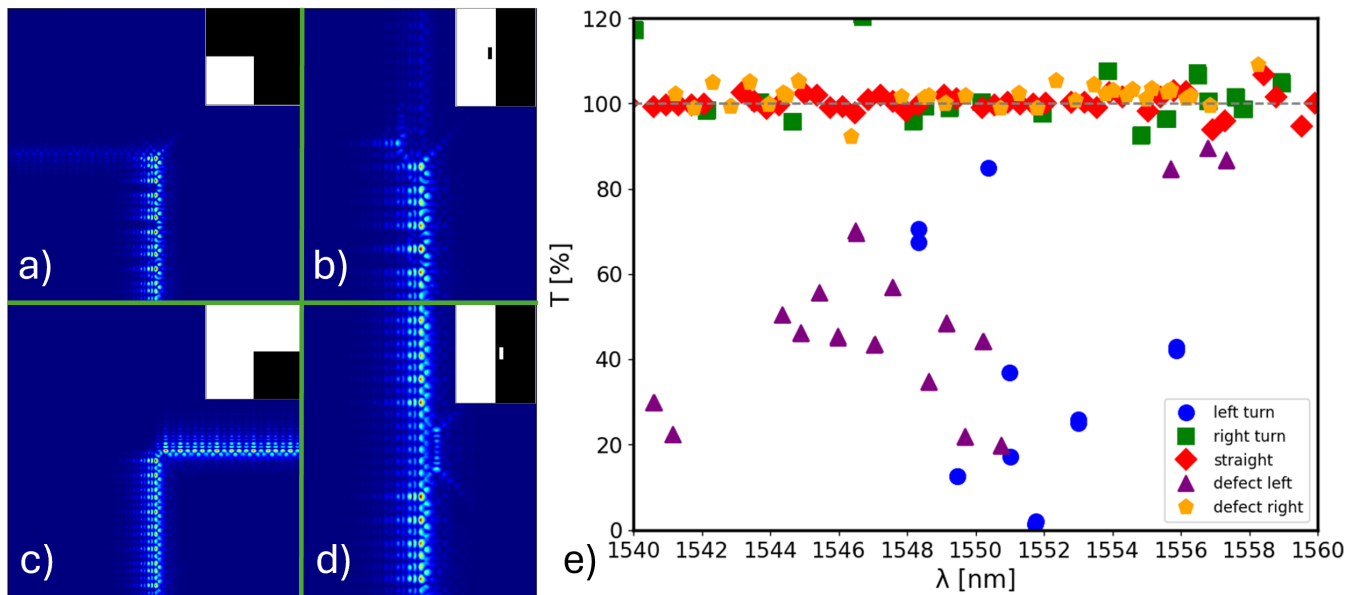


FIG. 4. a) Profile of  $E_z$  over left turn made out of design based on figure 3a. The black and white bitmap shows Inverted and Regular cells distribution. White represents regular cells, black represents Inverted cells. The simulation region is  $40 \times 40$  cells. b) Profile of  $E_z$  over defect on the left side of the interface, simulation  $25 \times 20$  cells. c) Profile of  $E_z$  over right turn, simulation  $40 \times 40$  cells. d) Profile of  $E_z$  over defect on the right side of the interface, simulation  $25 \times 20$  cells. e) Transmission of the topological modes of the elements in 4a-d centered around  $\lambda = 1550$  nm

example, in Figure 6a (with 6 periods), the field amplitude is only slightly higher around the second interface than the first, whereas in Figure 6b (with 14 periods), the mode is fully concentrated on the second interface.

This enhanced localization also stabilizes the topological bands: as shown in Figure 5b, increasing the number of periods causes the band positions to converge to a stable energy range. Therefore, the number of PC periods around the interface is a crucial design parameter for compact photonic devices, such as logic gates and couplers, where space is limited yet robust unidirectional transport is essential.

#### IV. CONCLUSION

We have designed a photonic crystal structure with the interface that supports partially  $\mathbb{Z}_2$ -protected topological modes, demonstrating a novel approach to leveraging partial band inversion to create states that mimic the topological protection of fully  $\mathbb{Z}_2$ -protected states. Our study utilized a real material commonly employed in photonics, which is well-suited for lithography, highlighting the practical applicability of our design. Furthermore, we targeted the topological modes to 1550 nm, a critical wavelength for telecommunications, underlining the relevance of this work for real-world applications.

In the waveguide regime, we observed 100% transmission, showcasing the lossless nature of the design, which enhances energy efficiency. This feature is particularly advantageous for photonic devices requiring minimal energy loss. While these states exhibit robust transmission, their behavior differs from fully  $\mathbb{Z}_2$ -protected states when encountering defects or

turns. Specifically, the transmission was unaffected by right turns and defects on the right side of the interface. However, left turns and defects on the left side of the interface caused a reduction in transmission, indicating a dependence on the side of the interface where perturbations occur.

Additionally, we examined the impact of the number of photonic crystal (PC) periods surrounding the interface on band conversion and energy flow. In our example, using 10 periods of each design around the interface achieved 99.7% of energy flowing in one direction, while increasing the surrounding cells to 12 improved this value to 99.99%. These findings suggest that optimizing the PC design around the interface can further enhance the directional control and robustness of energy flow.

#### ACKNOWLEDGMENTS

We acknowledge financial support from Projects No. PID2023-152225NB-I00, and Severo Ochoa MATRANS42 (No. CEX2023-001263-S) of the Spanish Ministry of Science and Innovation (Grant No. MICIU/AEI/10.13039/501100011033 and FEDER, EU), Projects No. TED2021-129857B-I00 and PDC2023-145824-I00, funded by MCIN/AEI/10.13039/501100011033 and European Union NextGeneration EU/PRTR and by the Generalitat de Catalunya (2021 SGR 00445, 2021 SGR 00804). We also acknowledge the financial support from the Charles University, project GA UK No. 80224 and the support provided by the Ferroic Multifunctionalities project, supported by the Ministry of Education, Youth, and Sports of the Czech

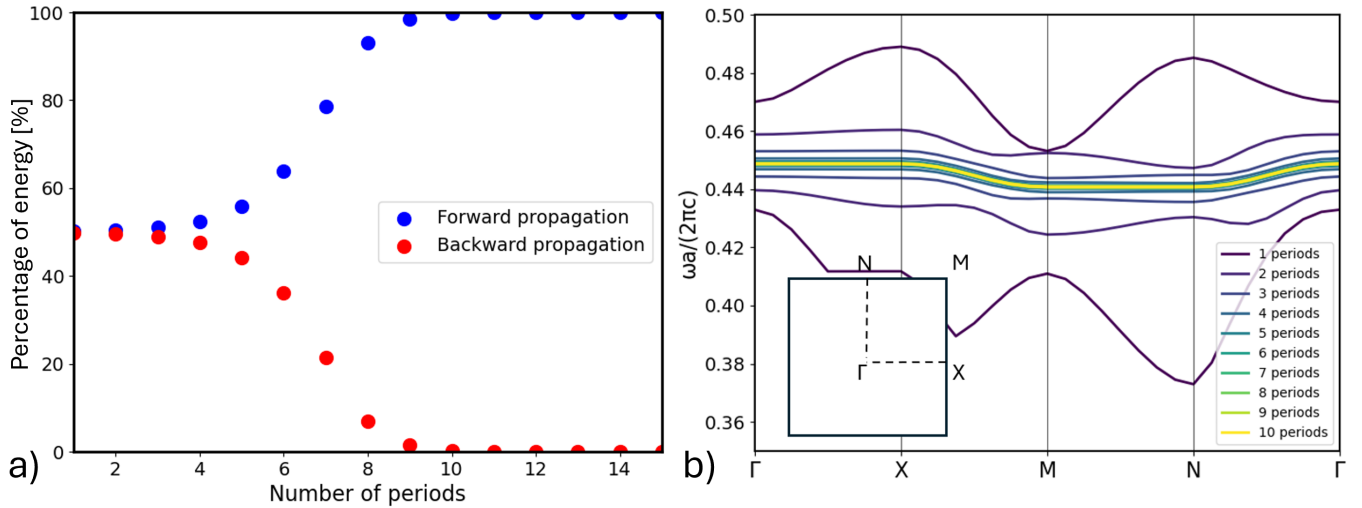


FIG. 5. a) Percentage of energy in the mode propagate in one direction as a function of number of cells around the interface based on design in figure 3a. b) Evolution of topological modes based on design from figure 3 with different number of periods around the interface.

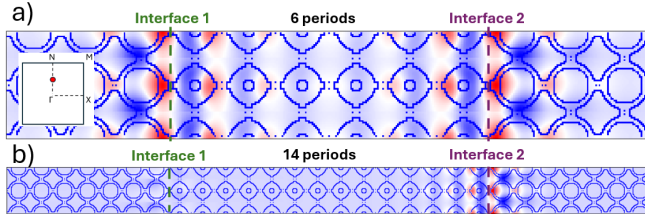


FIG. 6.  $E_z$  field distribution of an eigenmode of lower topological mode based on design from figure 3. a) Using 6 periods b) using 14 periods. The fields are calculated between the  $\Gamma$  and  $N$  points. The dark blue lines represents the outline of the geometrical structure. The outlines do not capture the structure perfectly. For a precise representation, refer to Figure 2c.

Republic [Project No. CZ.02.01.01/00/22\_008/0004591]

## DATA AVAILABILITY STATEMENT

The data that support the findings of this study are available from the corresponding author upon reasonable request.

## Appendix A: MPB calculations

For more details on MPB please visit the documentation <https://mpb.readthedocs.io/en/latest/>

### 1. Material model

At this date, MPB is not capable of model materials with dispersion. Material parameters can be anisotropic and complex (as long as the eigenvalues of the complex representation

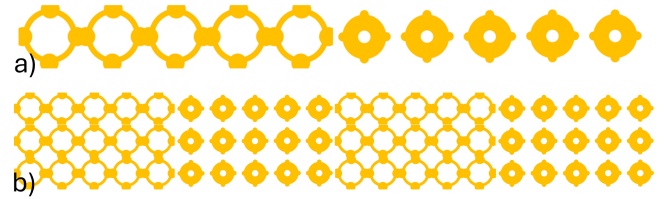


FIG. 7. Example of an interface construction in MPB. a) Elementary cell with 5 periods of each design, which will be periodically repeated. b) Combination of several elementary cells.

remains real, which is related to lossless materials), but there is no dependency on frequency.

For this reason, the calculated band structure is valid only for a region (y-axis) which corresponds to the wavelength at which the permittivity is defined. In our case, we use InP at 1550 nm, which corresponds to  $\epsilon_r = 10.01659$

This approximation is valid as it holds in the region of the PC band-gap and hence the topological states.

### 2. Interface simulations

MPB can calculate only periodical systems, which means that defining an interface as a boundary between two semi-infinite planes is not possible. In our calculations, we use several periods of the two complementary PC design as shown on figure 7a, which produces a pattern shown on fig. 7b. Using sufficient number of periods is required to simulate an interface between two PCs. In section III B we discussed, how the number of periods around the interface affects the formation of topological bands and their properties. It can also serve as a convergence test for the simulation validity. In ideal case, the number of periods  $N$  would be infinite, which would perfectly mimic the two semi-infinite PCs, but as we can see in figure

5, increasing  $N$  over 10 does not bring any noticeable change in properties of interest.

## Appendix B: FDTD simulations

We perform our FDTD simulations using Ansys Lumerical FDTD solver.

### 1. Material model

Unlike MPB, FDTD material model supports dispersion so this effect is already taken into account in transmission simulations. In FDTD, materials are modelled by polynomials over the spectral region of interest with Kramers–Kronig relations in mind. The dielectric tensor dispersion of the material model in our simulations is up to sixth polynomial order with no special weights for either real or imaginary part. In the simulation spectral region, the imaginary part of permittivity of InP is already negligible and we treat it as if it would be zero.

### 2. Topological source

In our simulations, we split the source preparation into two steps. In the first step, we used a combination of dipole sources with phase offset to evoke the topological modes in a straight interface and recorded the field at the other end of the interface. In the second step, we imported the recorded field as a new source in the simulation with the geometry that we want to investigate.

### 3. Boundary conditions

In contrast to MPB calculations, FDTD simulations do not use periodic boundary conditions. Instead, absorption layers are employed to prevent backscattering at the edges of the simulation region. This approach demonstrates that the results obtained from periodic MPB calculations are valid and translate well to finite systems.

### 4. Numerical oscillations

In figure 4e, it is apparent the transmission reaches values higher than 100% which is not physically correct. The problem is that the FDTD simulation operates in a time domain, which means that the spectral data are recorded by Fourier transformation. Since the length of the simulation is not infinite, the recorded data will be affected by oscillating error. This error is most apparent at the edges of the topological modes where the transmission sharply rises from 0 to 100%. Furthermore, since we are interested in transmission as a fraction of output field to input field, the oscillation in denominator causes further noise in the result. This fraction error is

apparent in 4e left turn and defect left data. After strong consideration, we decided that editing the data would only hurt the results. Cutting it to 100% would affect only the over-oscillations. Smoothing it would not help either, as some values might drastically overshoot and create a false impression of neighboring values being higher than they actually are. For this reason, we show this only as a qualitative demonstration rather than quantitative.

- <sup>1</sup>Sadao Adachi. Optical dispersion relations for gap, gasb, gasb, inp, inas, insb, al x ga1- x as, and in1- x ga x as y p1- y. *Journal of Applied Physics*, 66(12):6030–6040, 1989.
- <sup>2</sup>Sonakshi Arora, Thomas Bauer, Nikhil Parappurath, René Barczyk, Ewald Verhagen, and L Kuipers. Breakdown of spin-to-helicity locking at the nanoscale in topological photonic crystal edge states. *Physical Review Letters*, 128(20):203903, 2022.
- <sup>3</sup>B Andrei Bernevig and Shou-Cheng Zhang. Quantum spin hall effect. *Physical review letters*, 96(10):106802, 2006.
- <sup>4</sup>Maria Blanco de Paz, Chiara Devescovi, Geza Giedke, Juan José Saenz, Maia G Vergniory, Barry Bradlyn, Dario Bercioux, and Aitzol García-Etxarri. Tutorial: computing topological invariants in 2d photonic crystals. *Advanced Quantum Technologies*, 3(2):1900117, 2020.
- <sup>5</sup>Konstantin Y Bliokh, Daria Smirnova, and Franco Nori. Quantum spin hall effect of light. *Science*, 348(6242):1448–1451, 2015.
- <sup>6</sup>Chiara Devescovi, Antonio Morales-Pérez, Maria Blanco de Paz, Juan Luis Mañes, Barry Bradlyn, Maia G Vergniory, and Aitzol García-Etxarri. Tutorial 2.0: computing topological invariants in 3d photonic crystals. *Optical Materials Express*, 14(9):2161–2177, 2024.
- <sup>7</sup>Zongliang Du, Xianggui Ding, Hui Chen, Chang Liu, Weisheng Zhang, Jiachen Luo, and Xu Guo. Optimal design of topological waveguides by machine learning. *Frontiers in Materials*, 9:1075073, 2022.
- <sup>8</sup>Keita Funayama, Kenichi Yatsugi, Atsushi Miura, and Hideo Iizuka. Control of coupling between micromechanical topological waveguides. *International Journal of Mechanical Sciences*, 236:107755, 2022.
- <sup>9</sup>Yongkang Gong, Stephan Wong, Anthony J Bennett, Diana L Huffaker, and Sang Soon Oh. Topological insulator laser using valley-hall photonic crystals. *Acs Photonics*, 7(8):2089–2097, 2020.
- <sup>10</sup>Nils Valentin Hauff, Hanna Le Jeannic, Peter Lodahl, Stephen Hughes, and Nir Rotenberg. Chiral quantum optics in broken-symmetry and topological photonic crystal waveguides. *Physical Review Research*, 4(2):023082, 2022.
- <sup>11</sup>Liu He, Zhihao Lan, Yuting Yang, Qun Ren, Jian Wei You, Wei El Sha, Wu Liang, and Jianquan Yao. Wavelength division multiplexing based on the coupling effect of helical edge states in two-dimensional dielectric photonic crystals. *Optics Express*, 32(7):11259–11270, 2024.
- <sup>12</sup>Yi-Han He, Yong-Feng Gao, Hao-Zhe Lin, Meng-Cheng Jin, Yue He, and Xiao-Fei Qi. Topological edge and corner states based on the transformation and combination of photonic crystals with square lattice. *Optics Communications*, 512:128038, 2022.
- <sup>13</sup>Jing-Yu Huang, Xiao-Fang Xu, Hao Zhang, Nan Zhai, and Ya-Qi Liu. Topological boundary states of two-dimensional restricted isosceles triangular photonic crystals. *Applied Optics*, 61(5):1254–1260, 2022.
- <sup>14</sup>Umran S Inan and Robert A Marshall. *Numerical electromagnetics: the FDTD method*. Cambridge University Press, 2011.
- <sup>15</sup>Satoshi Iwamoto, Yasutomo Ota, and Yasuhiko Arakawa. Recent progress in topological waveguides and nanocavities in a semiconductor photonic crystal platform. *Optical Materials Express*, 11(2):319–337, 2021.
- <sup>16</sup>Dirk Jalas, Alexander Petrov, Manfred Eich, Wolfgang Freude, Shanhui Fan, Zongfu Yu, Roel Baets, Miloš Popović, Andrea Melloni, John D Joannopoulos, et al. What is—and what is not—an optical isolator. *Nature Photonics*, 7(8):579–582, 2013.
- <sup>17</sup>Meng-Cheng Jin, Yong-Feng Gao, Guang-Yao Huang, Yi-Han He, Jia-Ping Sun, and He Song. Manipulation of coupling between waveguide and ring resonator in topological photonic crystals. *Physica E: Low-dimensional Systems and Nanostructures*, 136:115013, 2022.
- <sup>18</sup>Steven G Johnson and John D Joannopoulos. Block-iterative frequency-domain methods for maxwell’s equations in a planewave basis. *Optics express*, 8(3):173–190, 2001.
- <sup>19</sup>Douglas Samuel Jones. *The theory of electromagnetism*. Elsevier, 2013.

- <sup>20</sup>Hibiki Kagami, Tomohiro Amemiya, Sho Okada, Nobuhiko Nishiyama, and Xiao Hu. Highly efficient vertical coupling to a topological waveguide with defect structure. *Optics Express*, 29(21):32755–32763, 2021.
- <sup>21</sup>Hibiki Kagami, Tomohiro Amemiya, Shou Okada, Nobuhiko Nishiyama, and Xiao Hu. Topological converter for high-efficiency coupling between si wire waveguide and topological waveguide. *Optics Express*, 28(22):33619–33631, 2020.
- <sup>22</sup>Juan Kang, Ruishan Wei, Qinglong Zhang, and Guoping Dong. Topological photonic states in waveguide arrays. *Advanced Physics Research*, 2(3):2200053, 2023.
- <sup>23</sup>O Kang-Hyok and Kwang-Hyon Kim. Multiband quadrupole topological photonic crystals with glide symmetries. *Optics & Laser Technology*, 168:109901, 2024.
- <sup>24</sup>Alexander B Khanikaev and Gennady Shvets. Two-dimensional topological photonics. *Nature photonics*, 11(12):763–773, 2017.
- <sup>25</sup>Mengyao Li, Ivan Sinev, Fedor Benimetskiy, Tatyana Ivanova, Ekaterina Khestanova, Svetlana Kiriushchikina, Anton Vakulenko, Sriram Guddala, Maurice Skolnick, Vinod M Menon, et al. Experimental observation of topological z2 exciton-polaritons in transition metal dichalcogenide monolayers. *Nature communications*, 12(1):4425, 2021.
- <sup>26</sup>Feng Liu, Hai-Yao Deng, and Katsunori Wakabayashi. Topological photonic crystals with zero berry curvature. *Physical Review B*, 97(3):035442, 2018.
- <sup>27</sup>Mo-Dian Liu, Hou-Hong Chen, Ziyu Wang, Yong Zhang, Xin Zhou, Guojing Tang, Fei Ma, Xin-Tao He, Xiao-Dong Chen, and Jian-Wen Dong. On-chip topological photonic crystal nanobeam filters. *Nano Letters*, 24(5):1635–1641, 2024.
- <sup>28</sup>Wenjing Liu, Minsoo Hwang, Zhurun Ji, Yuhui Wang, Gaurav Modi, and Ritesh Agarwal. Z2 photonic topological insulators in the visible wavelength range for robust nanoscale photonics. *Nano Letters*, 20(2):1329–1335, 2020.
- <sup>29</sup>Ling Lu, John D Joannopoulos, and Marin Soljačić. Topological photonics. *Nature photonics*, 8(11):821–829, 2014.
- <sup>30</sup>Joseph Maciejko, Taylor L Hughes, and Shou-Cheng Zhang. The quantum spin hall effect. *Annu. Rev. Condens. Matter Phys.*, 2(1):31–53, 2011.
- <sup>31</sup>Robert E Newnham. *Properties of materials: anisotropy, symmetry, structure*. Oxford university press, 2005.
- <sup>32</sup>Ardavan F Oskooi, David Roundy, Mihai Ibanescu, Peter Bermel, John D Joannopoulos, and Steven G Johnson. Meep: A flexible free-software package for electromagnetic simulations by the fdtd method. *Computer Physics Communications*, 181(3):687–702, 2010.
- <sup>33</sup>Tomoki Ozawa, Hannah M Price, Alberto Amo, Nathan Goldman, Mohammad Hafezi, Ling Lu, Mikael C Rechtsman, David Schuster, Jonathan Simon, Oded Zilberberg, et al. Topological photonics. *Reviews of Modern Physics*, 91(1):015006, 2019.
- <sup>34</sup>Mikael C Rechtsman. Reciprocal topological photonic crystals allow backscattering. *Nature Photonics*, 17(5):383–384, 2023.
- <sup>35</sup>Mikhail I Shalaev, Wiktor Walasik, and Natalia M Litchinitser. Optically tunable topological photonic crystal. *Optica*, 6(7):839–844, 2019.
- <sup>36</sup>Arvind K Sharma, Meghna Madhusudan, Steven M Burns, Parijat Mukherjee, Soner Yaldiz, Ramesh Harjani, and Sachin S Sapatnekar. Common-centroid layouts for analog circuits: Advantages and limitations. In *2021 Design, Automation & Test in Europe Conference & Exhibition (DATE)*, pages 1224–1229. IEEE, 2021.
- <sup>37</sup>Scott A Skirlo, Ling Lu, Yuichi Igarashi, Qinghui Yan, John Joannopoulos, and Marin Soljačić. Experimental observation of large chern numbers in photonic crystals. *Physical review letters*, 115(25):253901, 2015.
- <sup>38</sup>Daria Smirnova, Daniel Leykam, Yidong Chong, and Yuri Kivshar. Non-linear topological photonics. *Applied Physics Reviews*, 7(2), 2020.
- <sup>39</sup>Dennis M Sullivan. *Electromagnetic simulation using the FDTD method*. John Wiley & Sons, 2013.
- <sup>40</sup>Guo-Jing Tang, Xin-Tao He, Fu-Long Shi, Jian-Wei Liu, Xiao-Dong Chen, and Jian-Wen Dong. Topological photonic crystals: physics, designs, and applications. *Laser & Photonics Reviews*, 16(4):2100300, 2022.
- <sup>41</sup>Gregory Tkachov. *Topological insulators: The physics of spin helicity in quantum transport*. CRC Press, 2015.
- <sup>42</sup>Takanori Tsutaoka, Teruhiro Kasagi, and Kenichi Hatakeyama. Permeability spectra of yttrium iron garnet and its granular composite materials under dc magnetic field. *Journal of Applied Physics*, 110(5), 2011.
- <sup>43</sup>Hai-Xiao Wang and Jian-Hua Jiang. A short review of all-dielectric topological photonic crystals. *Frontiers in Physics*, 10:866552, 2022.
- <sup>44</sup>Hongfei Wang, Samit Kumar Gupta, Biye Xie, and Minghui Lu. Topological photonic crystals: a review. *Frontiers of Optoelectronics*, 13:50–72, 2020.
- <sup>45</sup>Zheng Wang, YD Chong, John D Joannopoulos, and Marin Soljačić. Reflection-free one-way edge modes in a gyromagnetic photonic crystal. *Physical review letters*, 100(1):013905, 2008.
- <sup>46</sup>Haruki Watanabe. A proof of the bloch theorem for lattice models. *Journal of Statistical Physics*, 177(4):717–726, 2019.
- <sup>47</sup>Junpeng Wu, Riyi Zheng, Jialuo Liang, Manzhou Ke, Jiuyang Lu, Weiyin Deng, Xueqin Huang, and Zhengyou Liu. Spin-dependent localization of helical edge states in a non-hermitian phononic crystal. *Physical Review Letters*, 133(12):126601, 2024.
- <sup>48</sup>Long-Hua Wu and Xiao Hu. Scheme for achieving a topological photonic crystal by using dielectric material. *Physical review letters*, 114(22):223901, 2015.
- <sup>49</sup>Langlang Xiong, Yufu Liu, Yu Zhang, Yaoxian Zheng, and Xunya Jiang. Topological properties of a two-dimensional photonic square lattice without c 4 and m x (y) symmetries. *Acs Photonics*, 9(7):2448–2454, 2022.
- <sup>50</sup>Lin Xu, Hai-Xiao Wang, Ya-Dong Xu, Huan-Yang Chen, and Jian-Hua Jiang. Accidental degeneracy in photonic bands and topological phase transitions in two-dimensional core-shell dielectric photonic crystals. *Optics express*, 24(16):18059–18071, 2016.
- <sup>51</sup>Shupeng Xu, Yuhui Wang, and Ritesh Agarwal. Absence of topological protection of the interface states in z 2 photonic crystals. *Physical Review Letters*, 131(5):053802, 2023.
- <sup>52</sup>Yuting Yang, Xinyue Qian, Liwei Shi, Xiaopeng Shen, Yifan Wang, and Zhi Hong Hang. Observation and control of pseudospin switching in a finite-width topological photonic crystal. *Optics Express*, 30(4):5731–5738, 2022.
- <sup>53</sup>Hironobu Yoshimi, Takuto Yamaguchi, Ryota Katsumi, Yasutomo Ota, Yasuhiko Arakawa, and Satoshi Iwamoto. Experimental demonstration of topological slow light waveguides in valley photonic crystals. *Optics Express*, 29(9):13441–13450, 2021.
- <sup>54</sup>Furong Zhang, Lu He, Huizhen Zhang, Ling-Jun Kong, Xingsheng Xu, and Xiangdong Zhang. Experimental realization of topologically-protected all-optical logic gates based on silicon photonic crystal slabs. *Laser & Photonics Reviews*, 17(8):2200329, 2023.
- <sup>55</sup>Qichen Zhang, Jianzhi Chen, Dongyang Liu, and Jianjun Liu. Topological states in penrose-square photonic crystals. *Journal of the Optical Society of America A*, 41(8):1611–1615, 2024.
- <sup>56</sup>Dmitry V Zhirihin and Yuri S Kivshar. Topological photonics on a small scale. *Small Science*, 1(12):2100065, 2021.